Original Article

Diagnostic accuracy of virtual non-calcium dual-energy computed tomography in the detection of acute occult ankle and calcaneus fractures

Ping Li^, Daobo Dong^, Feng Zhang, Jianguo Wang^, Hongxia Liu^

Department of Radiology, Affiliated Hospital of Shandong University of Traditional Chinese Medicine, Jinan, China

Contributions: (I) Conception and design: P Li, D Dong; (II) Administrative support: J Wang, H Liu; (III) Provision of study materials or patients: P Li, D Dong, F Zhang; (IV) Collection and assembly of data: All authors; (V) Data analysis and interpretation: P Li, D Dong, F Zhang, J Wang; (VI) Manuscript writing: All authors; (VII) Final approval of manuscript: All authors.

Correspondence to: Daobo Dong, BM. Department of Radiology, Affiliated Hospital of Shandong University of Traditional Chinese Medicine, No. 16369, Jingshi Road, Lixia District, Jinan 250014, China. Email: dongdaobo@126.com.

Background: Individuals with acute occult ankle and calcaneus fractures usually need to undergo additional magnetic resonance imaging (MRI) to confirm the diagnosis. In some cases, dual-energy computed tomography (DECT) is more convenient and efficient than MRI. This study aimed to assess the diagnostic accuracy of virtual non-calcium (VNCa) DECT in detecting acute occult ankle and calcaneus fractures.

Methods: From January 2022 to February 2024, adult patients presenting with ankle and calcaneal trauma but showing negative or inconclusive results on radiographs were enrolled in this prospective study. Ankle and calcaneus imaging was performed using DECT and MRI. Bone marrow edema (BME) was assessed by consolidating the MRI scan readings. Concurrently, the identification of fractures was conducted by consolidating the DECT and MRI scan readings. The computed tomography (CT) numbers corresponding to BME, fractures, and normal bone marrow in the VNCa images were compared. To determine the optimal cut-off CT number for ascertaining the presence or absence of BME and fractures, a receiver operating characteristic (ROC) curve analysis was conducted.

Results: The cohort comprised 180 participants (average age: 43±14 years; 92 male). In terms of BME detection, DECT had a sensitivity of 92% (96/104) and a specificity of 88% (67/76). In terms of fracture detection, DECT and MRI had a sensitivity of 95% (110/116) and 93% (108/116), respectively, and a specificity of 91% (58/64) and 92% (59/64), respectively. The optimal cut-off CT number for differentiating fractures from normal bone was 26.7 Hounsfield units (HU), which had a sensitivity of 97.3% (144/148) and a specificity of 100% (572/572).

Conclusions: Compared with MRI, VNCa imaging was found to be exceptionally accurate in diagnosing acute occult ankle and calcaneus fractures.

Keywords: Dual-energy computed tomography (DECT); virtual non-calcium (VNCa); magnetic resonance imaging (MRI); bone marrow edema (BME); occult ankle and calcaneus fractures

Submitted Oct 06, 2024. Accepted for publication Feb 13, 2025. Published online Mar 18, 2025.
doi: 10.21037/qims-24-2151
View this article at: https://dx.doi.org/10.21037/qims-24-2151

^ ORCID: Ping Li, 0000-0002-3842-4015; Daobo Dong, 0009-0004-5100-3292; Jianguo Wang, 0009-0007-2761-5565; Hongxia Liu, 0000-0002-4872-322X.

Introduction

Ankle fractures are increasingly common injuries, and the incidence of ankle fractures is increasing year by year (1). The primary causes of ankle fractures include falls, sports-related accidents, and traffic-related trauma (1,2). Without appropriate treatment, complications such as pain, osteoporosis, and traumatic osteoarthritis can develop (3,4). Therefore, the swift and accurate diagnosis of acute ankle or calcaneus fractures is crucial. However, certain fractures may go undetected in computed tomography (CT) images (5,6). Magnetic resonance imaging (MRI) has been shown to have distinct advantages in detecting bone marrow edema (BME) and occult fractures, including subtle trabecular fractures (7,8). However, despite its effectiveness, MRI is time consuming, costly, and potentially uncomfortable for fracture patients (9,10). In addition, the availability of MRI is limited in certain regions around the world, and MRI may not be covered by insurance. Further, patients with absolute or relative contraindications may not be able to safely undergo MRI scans.

Dual-energy CT (DECT) is a widely used clinical imaging technique (11) that can differentiate between materials (material decomposition). Virtual non-calcium (VNCa) imaging uses the principle of three substance separation to suppress high X-ray attenuation in trabecular bone. As a result, VNCa imaging can display subtle changes in the X-ray attenuation of bone marrow (12). Many previous studies have found no significant difference between VNCa imaging and MRI in detecting BME in various body parts, such as the spine, knee, ankle, foot, and scaphoid wrist (13-19). Extensive research has been conducted on the detection of occult fractures using MRI (20-22). However, few studies have explored the use of VNCa imaging for acute occult ankle and calcaneus fractures.

In this study, we posited that the diagnostic accuracy and confidence level for acute occult ankle and calcaneus fractures could be significantly enhanced through the use of color-coded VNCa images generated from third-generation dual-source DECT scans. The study aimed to prospectively compare DECT with MRI in adult participants afflicted with ankle or calcaneal trauma but exhibiting negative findings on radiographs. Specifically, this study aimed to: (I) assess the diagnostic accuracy of VNCa in visualizing BME, using the reading of MRI scans as the reference standard; and (II) compare the diagnostic accuracies of MRI and VNCa in the detection of fractures based on a combined reading of both MRI and DECT scans. We present this article in accordance with the STARD reporting checklist (available at https://qims.amegroups.com/article/view/10.21037/qims-24-2151/rc).

Methods

The study was conducted in accordance with the Declaration of Helsinki (as revised in 2013). This study was approved by the Ethics Committee of Shandong University of Traditional Chinese Medicine Affiliated Hospital (No. 2022096-KY). Before their inclusion in the study, all the participants provided their written informed consent.

Study participants

Patients from the Orthopedic Emergency Department, Microscopic Orthopedic Department, and Sports Orthopedic Departments of Shandong University of Traditional Chinese Medicine Affiliated Hospital were consecutively enrolled in this prospective study from January 2022 to February 2024. Adult patients aged 18 years and above, presenting with ankle and calcaneal trauma, and negative or inconclusive findings on radiographs, but a clinical suspicion of fracture were considered eligible for inclusion in the study (23). Patients were excluded from the study if they met any of the following exclusion criteria: had prior trauma or surgeries that could confound the analytical process; had multiple injuries that could pose a threat to their lives, or required emergency treatment (e.g., liver and spleen rupture); had conditions such as tumors, severe osteoarthritis, or systemic immune diseases that could adversely affect bone marrow appearance and density; had incomplete MRI or DECT imaging, impeding comparative evaluation; and/or had MRI scans displaying BME or fractures in both the ankle and calcaneus, precluding a side-by-side comparison of CT values on the VNCa images.

Definitions

In this study, on the VNCa images, BME was identified as a green area, while on the MRI images, BME was characterized by a higher signal intensity on fat suppression-T2 weighted imaging (FS-T2WI) and a lower signal intensity on T1 weighted imaging (T1WI). A fracture was characterized by cortical incongruence in two planes on the VNCa images, or as a linear or irregular BME extending to the cortex on the MRI images. Occult

fractures of the ankle or calcaneus included cases with both BME and fractures occurring at the distal tibia and fibula (within 3 cm of the joint surface), talus, or calcaneus.

Image acquisition

All the patients underwent DECT and MRI scans within 48 h of presenting with ankle or calcaneal trauma. The time difference between the two scanning modalities was kept below 12 h.

DECT protocol

The patients were placed in a supine position and scanned caudocranially by a dual-source DECT scanner (Somatom Force; Siemens Healthineers, Forchheim, Germany). The following protocol and parameters were used in the examination: low voltage tube 80 kV, 100 mAs, and high voltage tube Sn150 kV (Sn indicates the use of a 0.6 mm tin filter), and 150 mAs. An iterative reconstruction technique (ADMIRE, Siemens: strength level, 3) was employed, with a pitch of 0.7, a rotation time of 0.5 sec, and a volume CT dose index of 6.61 mGy. Transverse images were reconstructed with kernel Qr40 and Br59 (slice thickness: 0.6 mm; increment: 0.5 mm).

MRI protocol

The MRI scans were performed using a Signa 3.0T Pioneer (GE Healthcare, Chicago, USA), equipped with an adaptive coil primarily used for knees and ankles. The imaging protocol included axial FS-T2WI fast spin-echo (FSE) sequences [repetition time (TR)/echo time (TE): 4,005 ms/85 ms; echo train length: 16], sagittal FS-T2WI FSE sequence (TR/TE, 3,653 ms/85 ms; echo train length: 21), coronal FS-T2WI FSE sequence (TR/TE, 4,936 ms/110 ms; echo train length: 21), and coronal T1WI FSE sequence (TR/TE, 830 ms/111 ms; echo train length, 4). The thickness of all the MRI images was 3 mm.

Image postprocessing

The DECT images were processed on a commercial postprocessing workstation (syngo.via VB20-H3, Siemens Healthineers), where the VNCa series (Qr40) was calculated using the bone marrow application class [resolution: 4; minimum CT number: 100 Hounsfield units (HU); maximum CT number: 600 HU]. A color look-up table, part of syngo.via (bone marrow), was applied at a window width of 600 HU and a window level of 150 HU. Transverse, coronal, and sagittal VNCa images (slice thickness: 0.6 mm; increment: 0.5 mm) of the bilateral ankles and calcanei were calculated and saved in a color-coded format. Additionally, reconstructions were saved from the Br59 sharp kernel, with a 0.6 mm slice thickness and 0.5 mm increment in three planes.

Following reconstruction, the DECT and MRI images were transferred to a picture archiving and communication system (PACS) workstation (version 3.0.11.3; INFINITT PACS, Shanghai, China) for evaluation.

Image reading

The image assessment was performed on the PACS, with all the CT and MRI images assigned to the individual readers by a radiologist (F.Z., with 2 years of radiology experience) who did not participate in the image reading. Participant information remained undisclosed to all readers.

Four radiologists specializing in musculoskeletal radiology (i.e., D.D. with 20 years of experience; Yanyan Cheng with 15 years of experience; P.L. with 5 years of experience; and Xia Zhao with 10 years of experience) independently read the VNCa and MRI images. They scrutinized the distal ends of the tibia and fibula, talus, and calcaneus to determine the presence or absence of BME or fractures. Uncertain or ambiguous results were categorized as uncertain. Any discrepancy between the VNCa and MRI results was arbitrated by a consulting radiologist (J.W. with 30 years of experience in musculoskeletal radiology). Image quality, image noise, and diagnostic confidence were individually assessed using a 5-point Likert scale (ranging from 1–5; on which 1= unacceptable, and 5= excellent).

A sixth radiologist (H.L. with 30 years of experience in musculoskeletal imaging) performed a quantitative image analysis, measuring the CT numbers of BME and fractures on the axial color-coded VNCa images. The regions of interest (ROIs) were 0.3 cm^2 circles located in the center of the green area of the BME and the center of the yellow area of the suspected fracture on the VNCa images. The CT numbers of normal bone marrow at the contralateral symmetrical position were also measured and recorded.

The qualitative and quantitative data were analyzed by a statistician (Ning Cui with 20 years of experience in medical data statistics).

Radiation dose

The CT dose index volume (CTDIvol) and the dose-length product (DLP) were recorded. The effective dose was calculated as described previously (24).

Statistical analysis

The statistical computations were conducted using specialized software; that is, PASS for Win (version 15.0.5), SPSS Statistics for Windows (version 26.0, IBM), and MedCalc for Windows (version 15.6, MedCalc). The sample size was determined a priori to ensure that the sensitivity and specificity of DECT for detecting edema fell within a 95% confidence interval (CI) of 25%. A previous study reported sensitivity and specificity rates of 92% and 97%, respectively (13). Moreover, institutional data suggested that 93% of the participants would likely present with BME. Using the PASS15 software for calculations, a sample size of 180 participants was deemed adequate for non-inferiority testing.

Qualitative analysis

The baseline for evaluating BME was established based on the reading of the MRI scans. Fractures were assessed by employing the reference standard created by the combined reading of the MRI and DECT scans. Sensitivity, specificity, accuracy, and 95% CIs were calculated for individual bones (the bone level) and for each participant (the participant level) for both the DECT and MRI images. A participant was considered positive for fracture if the reader classified one of the imaged bones as a fracture or BME. The diagnostic accuracy of BME was calculated for DECT only, while the diagnostic accuracy of fractures was calculated for both MRI and DECT. Using the McNemar test, a P value <0.05 indicated a statistically significant difference (25). The inter-reader agreement for the BME and fracture ratings was calculated using Fleiss's κ. The Wilcoxon signed-rank test was employed for the subjective score data to compare diagnostic confidence, image quality, and image noise between the VNCa and MRI images. The inter-reader agreement was assessed by calculating weighted Fleiss's κ.

Quantitative analysis

A single-factor analysis of variance was used to compare the CT numbers of BME, fractures, and normal marrow on the VNCa images. A P value <0.05 indicated a statistically significant difference (26). A receiver operating characteristic (ROC) curve analysis and the area under the curve (AUC) were used to quantitatively evaluate the bone level CT numbers derived from the VNCa images, and to determine the optimal cut-off CT number for the presence or absence of BME or fractures that produced the highest accuracy. Sensitivity and specificity were calculated based on the cut-off CT number values.

Results

Initially, 188 participants were enrolled in the study, but eight participants were subsequently excluded (two because they had previously undergone ankle surgery; two because they could not undergo the MRI examination due to claustrophobia; and four because they declined the DECT examination for personal reasons) (*Figure 1*). The participants had a mean age ± standard deviation of 43±14 years, and an age range of 21–63 years; 92 of the 180 participants (51%) were male. The median time from trauma to the first scan was 5 h (interquartile range, 40 min–21 h). Almost half (49%; 88 of 180 participants) underwent MRI before DECT. The median time between the MRI and DECT scans was 2 h (interquartile range, 10 min–16 h) (*Table 1*).

In total, the study included 180 participants and 720 bones. Using the combined reading of the MRI scans, 136 bones (in 104 participants) were identified as having BME. By employing both MRI and DECT scans, fractures were confirmed in 148 bones (in 116 participants). BME was primarily found in the talus bones (80 bones), followed by the lateral malleolus (16), the medial malleolus (24), and the calcaneus (16). Fractures were most common in the lateral malleolus (64 bones), followed by the talus (24), the medial malleolus (16), the posterior malleolus (24), and the calcaneus (20). As *Figure 2* shows, the CT numbers of the affected (left) and healthy (right) sides differed significantly. BME and fractures failed to be observed on the X-ray radiograph. Traditional grayscale CT detected only 80 fracture lines without obvious displacement (52 lateral malleolus, 8 medial malleolus, 12 posterior malleolus, and 8 calcaneus). However, the VNCa, DECT, and MRI images clearly showed 180 BME and 164 fractures. *Figures 3*,*4* provide two examples of images of various modalities of occult fracture with peripheral BME.

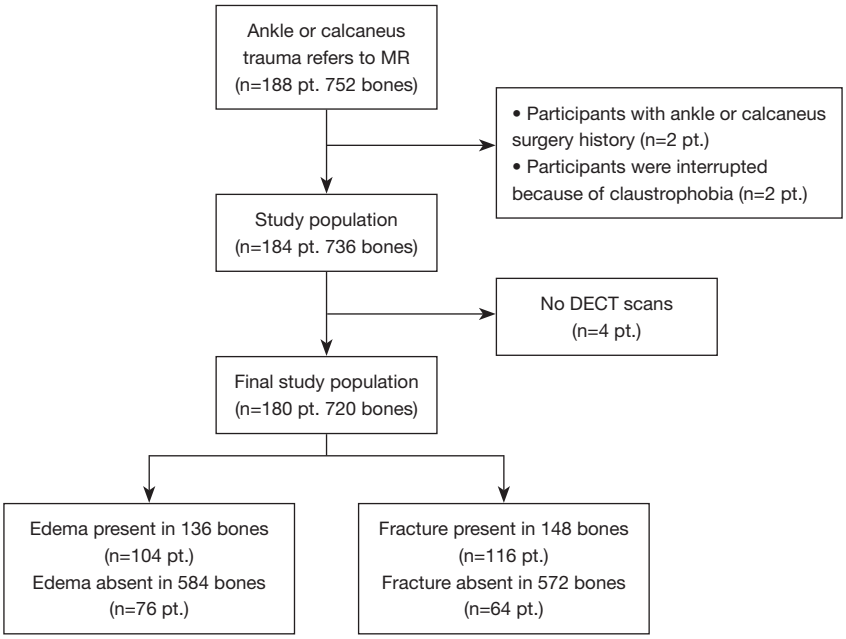

Figure 1 Flowchart showing the selection of the study population. In total, 188 study participants with clinical suspicion of ankle or calcaneus fractures but negative findings on radiographs were referred for MRI and DECT for further evaluation. All 188 participants were included in the final study population and underwent MRI and DECT. MR, magnetic resonance; pt., participants; MRI, magnetic resonance imaging; DECT, dual-energy computed tomography.

Table 1 Demographics of the participant population in this study

Parameter	Value
Number of participants	180
Age (years)	43±14
Males	92 [51]
Time between trauma and the first scan (h)	5 [2/3–21]
Time between MRI and DECT scans (h)	2 [1/6–16]
No. of ankles with MRI before DECT	88 [49]
No. of bones with BME per participant	
1	80
2	16
3	8
No. of bones with occult fractures per participant	
1	104
2	22

Data are presented as number, mean ± standard deviation, n [%], or median [interquartile range]. MRI, magnetic resonance imaging; DECT, dual-energy computed tomography; BME, bone marrow edema.

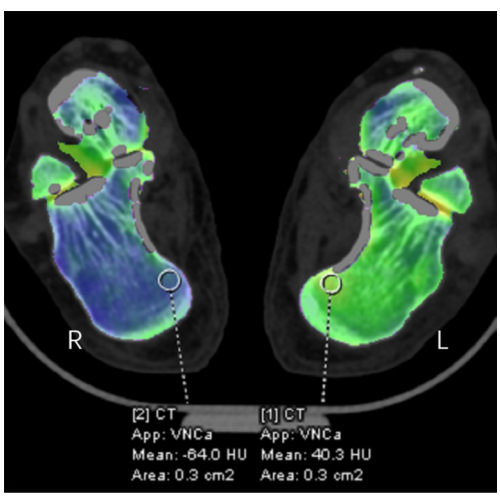

Figure 2 Bilateral calcaneal axial VNCa image. L: calcaneus fracture with a large BME area (calcaneal green or yellow-green area); R: calcaneus bone has normal bone marrow (purple area). 1 and 2 represent two ROIs of the same size and shape. 1 was placed in the central area of the fracture on the affected side, while 2 was placed in the symmetrical area on the healthy side. VNCa, virtual non-calcium; BME, bone marrow edema; ROIs, regions of interest; L, left; R, right.

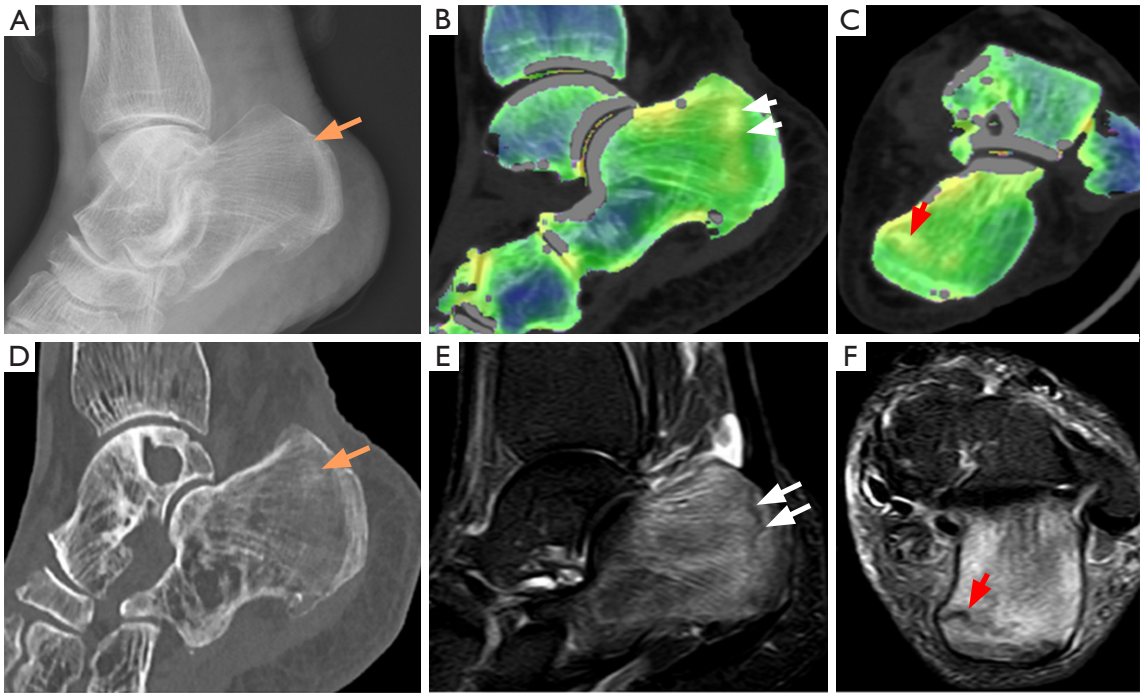

Figure 3 Images of a 64-year-old female with clinical suspicion of calcaneus fracture after trauma with negative findings on radiographs. X-ray radiography, MRI, and DECT scans were performed at 2, 6, and 7 h after the trauma, respectively. (A) No positive findings were observed on the X-ray radiograph (orange arrow). (B) Sagittal reformation of the DECT color-coded VNCa image of the left calcaneus showed a green area of BME and a yellow strip (white double arrows) of fracture. (C) Axial reformation of the DECT color-coded VNCa image of the left calcaneus showed a green area of BME and a yellow strip (red arrow) of fracture. (D) Conventional grayscale CT (Br59) showed the trabecular bone was slightly blurred (orange arrow), but no significant fracture line was observed. (E) Sagittal fat-suppression weighted imaging MRI scan of the left calcaneus showed significant BME and a clear fracture line (white double arrows). (F) Axial fat-suppression weighted imaging MRI scan of the left calcaneus showed significant BME and a clear fracture line (red arrow). MRI, magnetic resonance imaging; DECT, dual-energy computed tomography; VNCa, virtual non-calcium; BME, bone marrow edema; CT, computed tomography; Br, bone reconstruction algorithm.

Qualitative analysis

A qualitative image analysis was conducted to examine the diagnostic test accuracy of both modalities (*Tables 2,3*). At the bone level, BME detection had an accuracy of 97% (95% CI: 95–99%; 699 of 720 bones), a sensitivity of 88% (95% CI: 81–93%; 119 of 136 bones), and a specificity of 99% (95% CI: 98–100%; 580 of 584 bones). At the participant level, BME detection had an accuracy of 91% (95% CI: 85–94%; 163 of 180 participants), a sensitivity of 92% (95% CI: 85–97%; 96 of 104 participants), and a specificity of 88% (95% CI: 79–94%; 67 of 76 participants). Inter-reader consistency was exceptionally high, at 0.98, for both bone-level and participant-level evaluations.

In detecting fractures at the bone level, DECT had an accuracy of 98% (95% CI: 94–100%; 704 of 720 bones), while MRI had an accuracy of 97% (95% CI: 95–99%; 699 of 720 bones). At the bone level, DECT had a sensitivity of 95% (95% CI: 90–98%; 140 of 148 bones) and MRI had a sensitivity of 94% (95% CI: 89–97%; 139 of 148 bones). At the bone level, DECT had a specificity of 99% (95% CI: 97–99%; 564 of 572 bones), and MRI had a specificity of 98% (95% CI: 96–99%; 560 of 572 bones). The inter-reader consistency was high for both MRI (κ=0.98) and DECT (κ=0.98). At the participant level, DECT had an accuracy of 93% (95% CI: 88–96%; 168 of 180 participants), a sensitivity of 95% (95% CI: 89–98%; 110 of 160 participants), and a specificity of 91% (95% CI: 81–97%; 58 of 64 participants). At the participant level, MRI had an accuracy of 93% (95% CI: 88–96%; 167 of 180 participants), a sensitivity of 93% (95% CI: 83–97%; 108 of 116 participants), and a specificity of 92% (95%

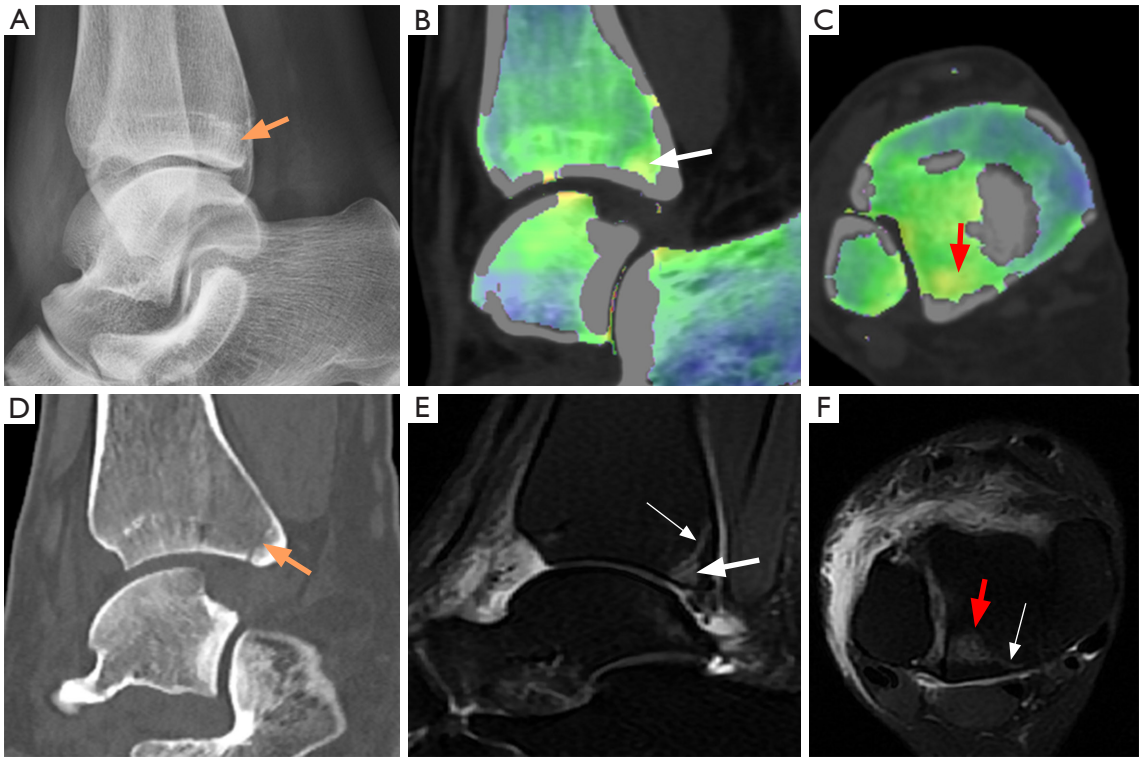

Figure 4 Images of a 37-year-old female who twisted her right ankle while descending stairs. X-ray radiography, MRI, and DECT were performed at 5, 6, and 8 h after trauma, respectively. (A) No positive results were observed on the X-ray image (orange arrow). (B) The sagittal reconstructions of the DECT color-coded VNCa image of the left posterior ankle revealed patchy yellow areas of BME (white single arrow). (C) The axial reconstructions of the DECT color-coded VNCa image of the left posterior ankle revealed patchy yellow areas of BME (red arrow). (D) Conventional grayscale CT (Br59) showed small and blurry low-density fracture lines (orange arrow) that were difficult to distinguish from vascular grooves. (E) The fracture line (white thin arrow) and axial bone marrow edema (white thick arrow) of the right posterior ankle on the MRI fat suppression images in the sagittal and axial directions. (F) The fracture line (white thin arrow) and axial bone marrow edema (red arrow) of the right posterior ankle on the MRI fat suppression images in the sagittal and axial directions. MRI, magnetic resonance imaging; DECT, dual-energy computed tomography; VNCa, virtual non-calcium; BME, bone marrow edema; CT, computed tomography; Br, bone reconstruction algorithm.

CI: 83–97%; 59 of 64 participants). The inter-reader consistency remained high for both MRI (κ=0.96) and DECT (κ=0.97). The McNemar test revealed no significant differences between MRI and DECT for any readers in the detection of fractures at either the participant or bone level (P=0.06 to >0.99).

Diagnostic confidence was high for all readers in the assessment of BME and fractures in the MRI series (mean score: 4.75±0.35) and VNCa images (mean score: 4.71±0.35), and no significant difference was found between the two modalities (P=0.13). The inter-reader agreement was moderate for the VNCa images (κ=0.75) and excellent for the MRI series (κ=0.81). There was no significant difference (P=0.08) between the reader ratings in terms of image noise in the MRI series (mean score 4.68±0.36) and VNCa images (mean score: 4.56±0.43). The inter-reader agreement was moderate for the VNCa images (κ=0.76) and excellent for the MRI series (κ=0.83). An assessment of image quality yielded mean scores of 4.79±0.33 (MRI series) and 4.74±0.32 (VNCa images), and no significant difference was found between the imaging modalities (P=0.38). The inter-reader agreement was moderate for the VNCa images (κ=0.73) and excellent for the MRI series (κ=0.85) (*Figure 5*).

Quantitative analysis

Significant differences were found in the CT numbers for BME, fractures, and normal bone marrow on the VNCa

Table 2 Diagnostic accuracy of DECT and MRI in determining BME in the ankle and calcaneus: bone level

Parameter	BME for DECT	Fractures for DECT	Fractures for MRI	P value for determining fractures*
Average of readers				0.38
Accuracy	97 (699/720) [95–99]	98 (704/720) [94–100]	97 (699/720) [95–99]	
Sensitivity	88 (119/136) [81–93]	95 (140/148) [90–98]	94 (139/148) [89–97]	
Specificity	99 (580/584) [98–100]	99 (564/572) [97–99]	98 (560/572) [96–99]	
Reader 1				0.69
Accuracy	95 (687/720) [89–98]	96 (692/720) [92–98]	95 (686/720) [89–98]	
Sensitivity	82 (112/136) [75–88]	89 (132/148) [83–94]	88 (130/148) [82–93]	
Specificity	98 (575/584) [97–99]	98 (560/572) [96–99]	97 (556/572) [96–98]	
Reader 2				0.38
Accuracy	98 (706/720) [96–99]	99 (711/720) [98–100]	98 (706/720) [96–99]	
Sensitivity	91 (124/136) [85–95]	98 (145/148) [94–100]	97 (144/148) [93–99]	
Specificity	99 (582/584) [99–100]	99 (566/572) [98–100]	98 (562/572) [97–99]	
Reader 3				0.69
Accuracy	97 (698/720) [95–99]	97 (696/720) [94–99]	96 (690/720) [92–98]	
Sensitivity	87 (118/136) [80–92]	91 (135/148) [85–95]	90 (133/148) [84–94]	
Specificity	99 (580/584) [98–100]	98 (561/572) [97–99]	97 (557/572) [96–99]	
Reader 4				0.06
Accuracy	98 (705/720) [96–100]	98 (704/720) [94–100]	97 (699/720) [95–99]	
Sensitivity	88 (119/136) [81–93]	95 (140/148) [90–98]	94 (139/148) [89–97]	
Specificity	99 (580/584) [98–100]	99 (564/572) [97–99]	98 (560/572) [96–99]	

The data represent the results of individual readers and the reader averages for DECT and MRI in determining BME or fractures in individual bones. The first numbers are percentages; the numbers in parentheses are numbers of bones (numerator over denominator); the numbers in brackets are 95% exact binomial confidence intervals. *, P values were obtained using the McNemar test to compare the rates of true cases for MRI and DECT in determining fractures. DECT, dual-energy computed tomography; MRI, magnetic resonance imaging; BME, bone marrow edema.

images (*Figure 6*). The optimal cut-off CT number for distinguishing between BME and normal bone marrow was 18.2 HU, with a sensitivity of 97.1% and a specificity of 81.8%. The overall AUC was 0.960 (95% CI: 0.92–0.983, P<0.001). The optimal cut-off CT number for distinguishing between fractures and normal bone marrow was 26.7 HU, with a sensitivity of 97.3% and a specificity of 100%. The overall AUC was 0.984 (95% CI: 0.89–1.00, P<0.001) (*Figure 7*).

Radiation

The mean CTDIvol was 5.2 mGy. The mean DLP was 89.6 mGycm. Using the factor κ=0.0004 as described previously (24), the mean effective dose was 0.035 mSv (range, 0.034–0.041 mSv, standard deviation =0.002 mSv).

Discussion

In recent years, the use of VNCa images in the diagnosis of musculoskeletal disorders has been increasing (27-31). Previous studies have suggested comparable diagnostic abilities between VNCa images and MRI images, particularly in identifying BME (13,14,18,19,32,33). However, few studies have examined acute occult fractures in the ankle and calcaneus. This study evaluated the effectiveness of MRI and

Table 3 Diagnostic accuracy of DECT and MRI in determining fractures in the ankle and calcaneus: participant level

Parameter	BME for DECT	Fractures for DECT	Fractures for MRI	P value for determining fractures*
Average of readers				0.63
Accuracy	91 (163/180) [85–94]	93 (168/180) [88–96]	93 (167/180) [88–96]	
Sensitivity	92 (96/104) [85–97]	95 (110/116) [89–98]	93 (108/116) [87–97]	
Specificity	88 (67/76) [79–94]	91 (58/164) [81–97]	92 (59/64) [83–97]	
Reader 1				0.13
Accuracy	87 (157/180) [81–92]	89 (161/180) [83–93]	88 (159/180) [83–93]	
Sensitivity	88 (92/104) [81–94]	91 (106/116) [85–96]	89 (103/116) [82–94]	
Specificity	86 (65/76) [76–93]	86 (55/64) [75–93]	88 (56/64) [77–94]	
Reader 2				0.50
Accuracy	93 (167/180) [88–96]	96 (173/180) [92–98]	96 (173/180) [92–98]	
Sensitivity	94 (98/104) [84–96]	97 (112/116) [91–99]	97 (112/116) [91–99]	
Specificity	91 (69/76) [82–96]	95 (61/64) [87–99]	92 (59/64) [83–97]	
Reader 3				0.29
Accuracy	88 (159/180) [82–92]	91 (163/180) [85–94]	87(157/180) [81–92]	
Sensitivity	91 (95/104) [84–96]	92 (107/116) [86–96]	88 (102/116) [81–93]	
Specificity	84 (64/76) [74–92]	88 (56/64) [77–94]	86 (55/64) [75–93]	
Reader 4				>0.99
Accuracy	94 (169/180) [89–97]	97 (175/180) [94–99]	98 (176/180) [94–99]	
Sensitivity	95 (99/104) [89–98]	97 (113/116) [93–100]	98 (114/116) [94–100]	
Specificity	92 (70/76) [84–97]	97 (62/64) [89–100]	97 (62/64) [89–100]	

The data are results of individual readers and reader averages for DECT and MRI in determining BME or fractures at each participant. The first numbers are percentages; the numbers in parentheses are the numbers of participants (numerator over denominator); the numbers in brackets are 95% exact binomial confidence intervals. *, P values were obtained using the McNemar test to compare the rates of true cases for MRI and DECT in determining fractures. MRI, magnetic resonance imaging; DECT, dual-energy computed tomography; BME, bone marrow edema.

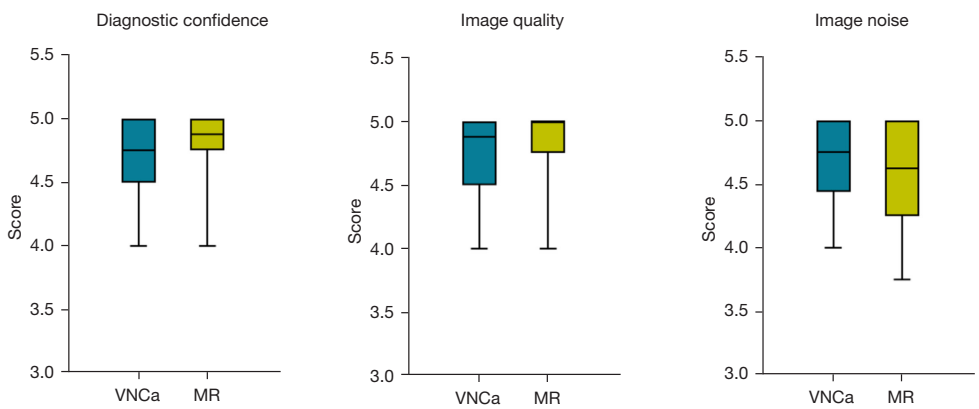

Figure 5 Box plots illustrating subjective image ratings in terms of diagnostic confidence, image quality, and image noise for MRI and color-coded VNCa imaging using 5-point Likert scales (ranging from 1–5, on which 1= unacceptable, and 5= excellent). The blue and yellow box diagrams represent subjective VNCa and MRI scores, respectively. The color-coded VNCa images and MRI series produced similar scores without significant differences in terms of diagnostic confidence (P=0.13), image quality (P=0.38), and image noise (P=0.08). The boxes show the upper and lower quartiles; the horizontal lines in the boxes indicate the median values; and the whiskers indicate the ranges. MR, magnetic resonance; MRI, magnetic resonance imaging; VNCa, virtual non-calcium.

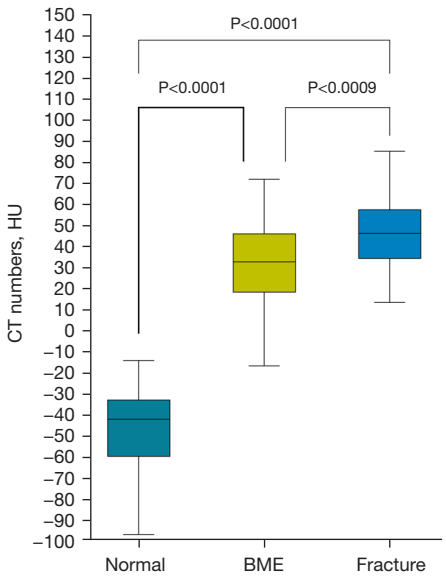

Figure 6 Box plot of the CT numbers for BME, fractures, and normal bone marrow. Normal bone marrow, BME, and fractures represent the CT numbers of the normal bone marrow, the affected side with BME, and the fractures on the VNCa images, respectively. The quantitative image analysis showed a significant difference in the CT numbers between BME and normal bone marrow (P<0.0001). The CT values of BME and fracture also differed significantly (P=0.0009). The boxes show the upper and lower quartiles; the horizontal lines in the boxes indicate median numbers; and the whiskers indicate ranges. The median CT numbers of BME, fracture, and normal bone marrow were 33, 46.6, and −41.6 HU, respectively. The upper quartiles of BME, fracture, and normal bone marrow were 46.37, 57.8, and −32.5 HU, respectively, and the lower quartiles were 18.68, 34.8, and −58.9 HU, respectively. The maximum numbers of BME, fracture, and normal bone marrow were 72.3, 85.5, and −13 HU, respectively, and the corresponding minimum numbers were −16.3, 13.8, and −96.3 HU, respectively. CT, computed tomography; BME, bone marrow edema; VNCa, virtual non-calcium; HU, Hounsfield unit.

DECT in diagnosing acute traumatic BME and fractures in the ankle and calcaneus. Our findings highlighted the robust sensitivity, specificity, and accuracy of VNCa images in identifying bones with BME and fractures at both the bone and participant levels. The McNemar test revealed no significant discrepancies between the two modalities in terms of their efficacy in detecting ankle and calcaneus fractures both for individual readers and collectively (P=0.06 to >0.99). These insights could help radiologists to diagnose occult injuries in the ankle and calcaneus swiftly and accurately, thereby facilitating efficient treatment strategies (e.g., immobilization, external fixation, and clinical bone injury medication treatment) by orthopedists, and preventing greater trauma, osteoporosis, or osteoarthritis due to neglect.

Our research represents a marked improvement in the detection of both BME and fractures compared with previous studies (34,35). This improvement is primarily attributable to advancements in medical equipment. The first generation dual-source DECT imaging only had one kV selection of 80/140 kV. A 0.4-mm tin filter was added to the second generation dual-source CT, which raised the level of high-energy radiation by one level. In the third generation dual-source CT, two sets of X-ray tubes and detector systems are used to work synchronously, greatly improving the scanning speed. By separating and integrating two sets of data with different energies, higher quality images can be obtained (36). The sensitivity for BME detection was somewhat lower than that for fractures; however, this can be explained by the variability in bone marrow density across the tibial plafond, malleolus, and talar body or head in the ankle joint—a factor that contributes to false positives in BME evaluations (35). In contrast to Müller *et al.*'s findings (19), our study found that VNCa imaging showed superior sensitivity in detecting both BME and fractures at both the participant- and bone-specific levels. The variations in the anatomical locations, sizes, and shapes of the bones examined in the study might account for this discrepancy. Further, previous research has suggested that VNCa imaging may exhibit poorer sensitivity in identifying BME in smaller bones (31). Our study employed a maximum CT number of 600 HU and a threshold CT number of 100 HU, effectively reducing the occurrence of false positives.

In the quantitative analysis, we compared the CT numbers from affected regions with their symmetrical contralateral ROIs, distinguishing between the differences in the CT numbers for BME, fractures, and normal bone marrow. Our measurements slightly exceeded those reported by Koch *et al.* (18), which could be attributed to the shorter time interval between the traumatic event and the DECT scans. Fresh bleeding density, consequential to fractures, may explain the elevated density visible in the affected regions on VNCa images (37). Additionally, a large proportion of our study participants were younger, resulting in bones with higher hydroxyapatite and magnesium content, factors contributing to higher CT numbers (38,39). Moreover, our data showed considerable variability in the CT numbers

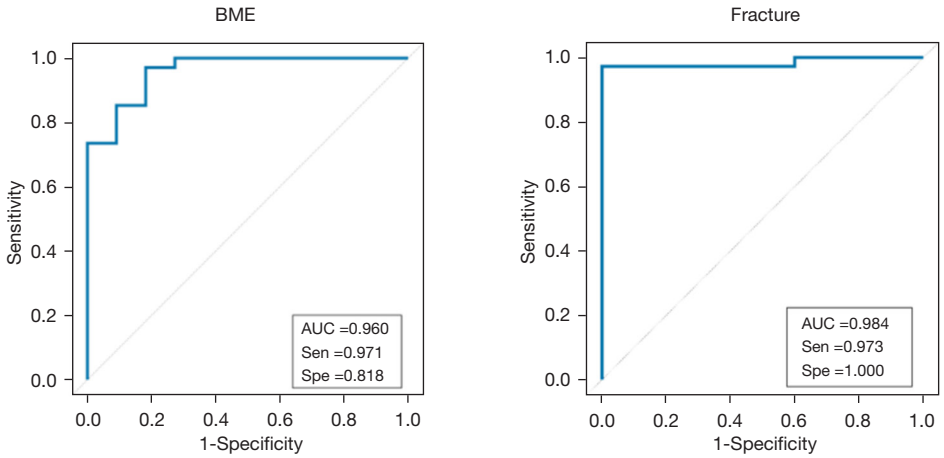

Figure 7 Representative ROC curve for BME derived from CT numbers on VNCa images in 134 bones. The overall AUC was 0.960 (95% CI: 0.855–1.000, P<0.001). The sensitivity was 97.1%, and the specificity was 81.8%. The representative ROC curve for fracture was derived from CT numbers on VNCa images in 138 bones. The overall AUC was 0.984 (95% CI: 0.887–1.000, P<0.001). The sensitivity was 97.3%, and the specificity was 100.0%. ROC, receiver operating characteristic; BME, bone marrow edema; CT, computed tomography; VNCa, virtual non-calcium; AUC, area under the curve; CI, confidence interval; Sen, sensitivity; Spe, specificity.

for BME and fractures, which could be due to the varying extents of trabecular bone fractures. These fractures may induce more bleeding, consequently elevating the VNCa image CT numbers (37,40).

This study had a number of limitations. First, fixing the size of the ROI might have influenced the recorded CT numbers in the ROI. We intend to address this issue in future studies by adjusting the ROI size according to the extent of the BME. Second, a negligible subset of both the MRI and DECT images displayed BME resulting from osteochondral injuries. Despite their inclusion, these images did not significantly affect our overall findings. Third, scanning both ankles and calcanei escalates participant radiation exposure, an aspect warranting further investigation. Further, the production of artifacts, particularly in smaller bones by VNCa imaging, remains an issue for future technological refinement. Finally, our findings, specifically the proposed CT number thresholds, may not apply to equipment from different manufacturers or diverse processing platforms.

Conclusions

In conclusion, VNCa imaging showed excellent sensitivity, specificity, and accuracy in detecting radiographically negative ankle and calcaneus fractures, and did not differ significantly from MRI. If MRI is unavailable, contraindicated, or in emergency cases, VNCa imaging may serve as a convenient alternative for examinations.

Acknowledgments

None.

Footnote

Reporting Checklist: The authors have completed the STARD reporting checklist. Available at https://qims.amegroups.com/article/view/10.21037/qims-24-2151/rc

Funding: None.

Conflicts of Interest: All authors have completed the ICMJE uniform disclosure form (available at https://qims.amegroups.com/article/view/10.21037/qims-24-2151/coif). The authors have no conflicts of interest to declare.

Ethical Statement: The authors are accountable for all aspects of the work in ensuring that questions related to the accuracy or integrity of any part of the work are appropriately investigated and resolved. The study was conducted in accordance with the Declaration of Helsinki (as revised in 2013). This study was approved by the Ethics Committee of Shandong University of Traditional Chinese Medicine Affiliated Hospital (No. 2022096-KY). Before their inclusion in the study, all the participants provided

their written informed consent.

References

1. Kang HJ, Lee JW, Kwon YM, Kim SJ. Epidemiology of Ankle Fractures in Korea: A Nationwide Population-Based Study. J Korean Med Sci 2022;37:e288.
2. Hansen R, Shibuya N, Jupiter DC. An Updated Epidemiology of Foot and Ankle Fractures in the United States: Complications, Mechanisms, and Risk Factors. J Foot Ankle Surg 2022;61:1034-8.
3. Khlopas H, Khlopas A, Samuel LT, Ohliger E, Sultan AA, Chughtai M, Mont MA. Current Concepts in Osteoarthritis of the Ankle: Review. Surg Technol Int 2019;35:280-94.
4. Jantzen C, Ebskov LB, Andersen KH, Benyahia M, Rasmussen PB, Johansen JK. Ankle arthrosis. Ugeskr Laeger 2020;182:V04200244.
5. Davidson A, Silver N, Cohen D, Gross M, Zinger G, Applbaum Y, Lebel E, Peyser A. Justifying CT prior to MRI in cases of suspected occult hip fracture. A proposed diagnostic protocol. Injury 2021;52:1429-33.
6. Jiang JZ, Zhang MR, Huang PK, Huang LS. CT imaging features and misdiagnosis analysis of occult anterior calcaneal process fracture. Zhongguo Gu Shang 2019;32:1057-62.
7. Foex BA, Russell A. BET 2: CT versus MRI for occult hip fractures. Emerg Med J 2018;35:645-7.
8. Buturoiu MM, Ghiea S, Weber MA. Subchondral insufficiency fractures: overview of MRI findings from hip to ankle joint. Rofo 2024;196:1143-54.
9. Teixeira PAG, Kessler H, Morbée L, Douis N, Boubaker F, Gillet R, Blum A. Mineralized tissue visualization with MRI: Practical insights and recommendations for optimized clinical applications. Diagn Interv Imaging 2024. [Epub ahead of print] doi: 10.1016/j.diii.2024.11.001.
10. Lebel K, Mondesert B, Robillard J, Pham M, Terrone D, Tan S. 2020 MR Safety for Cardiac Devices: An Update for Radiologists. Can Assoc Radiol J 2021;72:814-30.
11. D'Angelo T, Albrecht MH, Caudo D, Mazziotti S, Vogl TJ, Wichmann JL, Martin S, Yel I, Ascenti G, Koch V, Cicero G, Blandino A, Booz C. Virtual non-calcium dual-energy CT: clinical applications. Eur Radiol Exp 2021;5:38.
12. Gosangi B, Mandell JC, Weaver MJ, Uyeda JW, Smith SE, Sodickson AD, Khurana B. Bone Marrow Edema at Dual-Energy CT: A Game Changer in the Emergency Department. Radiographics 2020;40:859-74.
13. François MA, Comby PO, Goueslard K, Lebeaupin F, Lemogne B, Ricolfi F, Lenfant M. Diagnostic performance of spectral CT in detecting bone marrow edema for vertebral fracture: A multi-reader study. Eur J Radiol 2025;182:111857.
14. Mens MA, de Geus A, Wellenberg RHH, Streekstra GJ, Weil NL, Bus SA, Busch-Westbroek TE, Nieuwdorp M, Maas M. Preliminary evaluation of dual-energy CT to quantitatively assess bone marrow edema in patients with diabetic foot ulcers and suspected osteomyelitis. Eur Radiol 2023;33:5645-52.
15. Lu H, Li Z, Liang Z, Liu Y. Diagnostic efficacy of dual-energy CT virtual non-calcium technique in the diagnosis of bone marrow edema of sacroiliac joints in ankylosing spondylitis. J Orthop Surg Res 2025;20:28.
16. Fang Y, Liu C, Yu W, Zhan Y, Li W, Liang J, Hong G. Dual-energy CT Virtual Non-Calcium Image is Beneficial for the Detection of Non-displaced Knee Fractures. Curr Med Imaging 2023;19:1178-85.
17. Foti G, Guerriero M, Faccioli N, Fighera A, Romano L, Zorzi C, Carbognin G. Identification of bone marrow edema around the ankle joint in non-traumatic patients: Diagnostic accuracy of dual-energy computed tomography. Clin Imaging 2021;69:341-8.
18. Koch V, Müller FC, Gosvig K, Albrecht MH, Yel I, Lenga L, Martin SS, Cavallaro M, Wichmann JL, Mader C, D'Angelo T, Mazziotti S, Cicero G, Vogl TJ, Booz C. Incremental diagnostic value of color-coded virtual non-calcium dual-energy CT for the assessment of traumatic bone marrow edema of the scaphoid. Eur Radiol 2021;31:4428-37.
19. Müller FC, Gosvig KK, Børgesen H, Gade JS, Brejnebøl M, Rodell A, Nèmery M, Boesen M. Dual-Energy CT for Suspected Radiographically Negative Wrist Fractures: A Prospective Diagnostic Test Accuracy Study. Radiology 2020;296:596-602.
20. Heynen B, Tamigneaux C, Pasoglou V, Malghem J, Vande Berg B, Kirchgesner T. MRI detection of radiographically occult fractures of the hip and pelvis in the elderly: Comparison of T2-weighted Dixon sequence with T1-

weighted and STIR sequences. Diagn Interv Imaging 2019;100:169-75.
21. Akkemik Ö, Kugel H, Fischbach R. Acute soft tissue injury to the temporomandibular joint and posttraumatic assessment after mandibular condyle fractures: a longitudinal prospective MRI study. Dentomaxillofac Radiol 2022;51:20210148.
22. Jarrett DY, Kramer DE, Laor T. Magnetic resonance imaging of medial collateral ligament avulsion fractures of the knee in children: a potentially underestimated injury. Pediatr Radiol 2021;51:1705-13.
23. Stiell I. Ottawa ankle rules. Can Fam Physician 1996;42:478-80.
24. Saltybaeva N, Jafari ME, Hupfer M, Kalender WA. Estimates of effective dose for CT scans of the lower extremities. Radiology 2014;273:153-9.
25. McNEMAR Q. Note on the sampling error of the difference between correlated proportions or percentages. Psychometrika 1947;12:153-7.
26. Mishra P, Singh U, Pandey CM, Mishra P, Pandey G. Application of student's t-test, analysis of variance, and covariance. Ann Card Anaesth 2019;22:407-11.
27. Singla N, Joshi M, Amerasekera S, Choudhary S. Applications of dual-energy CT in acute musculoskeletal and trauma imaging-a review. Skeletal Radiol 2024;53:2333-45.
28. Fervers P, Celik E, Bratke G, Maintz D, Baues C, Ruffing S, Pollman-Schweckhorst P, Kottlors J, Lennartz S, Große Hokamp N. Radiotherapy Response Assessment of Multiple Myeloma: A Dual-Energy CT Approach With Virtual Non-Calcium Images. Front Oncol 2021;11:734819.
29. Zuo T, Chen Y, Zheng H, Jia X, Bao Y, Wang Y, Li L, Huang X. Detection of bone marrow edema in osteonecrosis of the femoral head using virtual noncalcium dual-energy computed tomography. Eur J Radiol 2021;139:109681.
30. Koch V, Albrecht MH, Gruenewald LD, Yel I, Eichler K, Gruber-Rouh T, Hammerstingl RM, Burck I, Wichmann JL, Alizadeh LS, Vogl TJ, Lenga L, Mader C, Martin SS, Mazziotti S, D'Angelo T, Booz C. Diagnostic accuracy of color-coded virtual noncalcium reconstructions derived from portal venous phase dual-energy CT in the assessment of lumbar disk herniation. Eur Radiol 2022;32:2168-77.
31. Yan YY, Ouellette HA, Saththianathan M, Munk PL, Mallinson PI, Sheikh A. The Role of a Virtual Noncalcium Dual-Energy CT Application in the Detection of Bone Marrow Edema in Peripheral Osteomyelitis. Can Assoc Radiol J 2022;73:549-56.
32. Ahmad MI, Liu L, Sheikh A, Nicolaou S. Dual-energy CT: Impact of detecting bone marrow oedema in occult trauma in the Emergency. BJR Open 2024;6:tzae025.
33. Foti G, Sanfilippo L, Longo C, Oliboni E, De Santis N, Iacono V, Serra G, Guerriero M, Filippini R. Diagnostic Accuracy of Dual-Energy CT for Bone Stress Injury of the Lower Limb. Radiology 2024;313:e232415.
34. Guggenberger R, Gnannt R, Hodler J, Krauss B, Wanner GA, Csuka E, Payne B, Frauenfelder T, Andreisek G, Alkadhi H. Diagnostic performance of dual-energy CT for the detection of traumatic bone marrow lesions in the ankle: comparison with MR imaging. Radiology 2012;264:164-73.
35. Pache G, Krauss B, Strohm P, Saueressig U, Blanke P, Bulla S, Schäfer O, Helwig P, Kotter E, Langer M, Baumann T. Dual-energy CT virtual noncalcium technique: detecting posttraumatic bone marrow lesions--feasibility study. Radiology 2010;256:617-24.
36. Goo HW, Goo JM. Dual-Energy CT: New Horizon in Medical Imaging. Korean J Radiol 2017;18:555-69.
37. Cottrell JA, Turner JC, Arinzeh TL, O'Connor JP. The Biology of Bone and Ligament Healing. Foot Ankle Clin 2016;21:739-61.
38. Pathria MN, Chung CB, Resnick DL. Acute and Stress-related Injuries of Bone and Cartilage: Pertinent Anatomy, Basic Biomechanics, and Imaging Perspective. Radiology 2016;280:21-38.
39. Karampinos DC, Ruschke S, Dieckmeyer M, Diefenbach M, Franz D, Gersing AS, Krug R, Baum T. Quantitative MRI and spectroscopy of bone marrow. J Magn Reson Imaging 2018;47:332-53.
40. Bahney CS, Zondervan RL, Allison P, Theologis A, Ashley JW, Ahn J, Miclau T, Marcucio RS, Hankenson KD. Cellular biology of fracture healing. J Orthop Res 2019;37:35-50.

Cite this article as: Li P, Dong D, Zhang F, Wang J, Liu H. Diagnostic accuracy of virtual non-calcium dual-energy computed tomography in the detection of acute occult ankle and calcaneus fractures. Quant Imaging Med Surg 2025;15(4):2839-2851. doi: 10.21037/qims-24-2151

